Optimization of the UNRES Force Field by Hierarchical Design of the Potential-Energy Landscape. 1. Tests of the Approach Using Simple Lattice Protein Models

Adam Liwo,[†,‡] Piotr Arłukowicz,[‡] Stanisław Ołdziej,[†,‡] Cezary Czaplewski,[†,‡] Mariusz Makowski,[†,‡] and Harold A. Scheraga*[,†]

Baker Laboratory of Chemistry and Chemical Biology, Cornell University, Ithaca, New York 14853-1301, and Faculty of Chemistry, University of Gdańsk, Sobieskiego 18, 80-952 Gdańsk, Poland

Received: April 30, 2004; In Final Form: August 12, 2004

In this and two accompanying papers, we report the development of our recently proposed method for optimizing potential-energy functions for protein-structure prediction and folding simulations (Liwo, A.; Arłukowicz, P.; Czaplewski, C.; Ołdziej, S.; Pillardy, J.; Scheraga, H. A. *Proc. Natl. Acad. Sci. U.S.A.* **2002**, *99*, 1937−1942) aimed at obtaining hierarchical energy landscapes of the protein(s) chosen to calibrate a force field (in which the free energy decreases with increasing degree of nativelikeness). The structure of each benchmark protein is described in terms of structural levels, the number of native structural elements increasing in a given order with level number. Optimization is aimed at lowering the free energy with increasing level of the structural hierarchy. In this paper, we implemented cubic-lattice models of 12-bead polypeptide chains to study the properties of the method and to assess its advantage over a single energy gap and *Z*-score optimization. The interaction potential consisted of the hydrophobic-polar HP-type potential, a contact potential for peptide-group interaction (simulating hydrogen bonding), and a local potential consisting of bending and torsional terms. Canonical Monte Carlo simulations were carried out at various temperatures for each of several systems and with each of several sets of energy-function parameters to determine the stability (τ_s^{max}) and the folding time (τ_f^{min}). We found that, with moderate energy gaps, nonhierarchical optimization results in both poor (resulting in large τ_f^{min} and small τ_s^{max}) and good (resulting in small τ_f^{min} and large τ_s^{max}) folders, whereas increasing the energy gap improves the folding properties. Good folders are characterized by low-energy structures with some nativelike elements and high-energy states with no native elements, whereas the reverse is true for poor folders. Subsequently, hierarchical optimizations were carried out with various hierarchies, starting by assembling more and more nativelike elements with increasing level number and then carefully considering the folding pathway. We found that explicit introduction of an appropriate structural hierarchy into the optimization procedure substantially improves foldability; however, a wrongly designed hierarchy can impair it. We also found that the best ordering should follow the most efficient path to the native structure, without creating low-energy intermediates separated by large energy barriers. For an appropriate hierarchy, τ_f^{min} is low, and τ_s^{max} increases with the energy gap, which reflects the increased thermodynamic stability of the native structure. It was also found that an analysis of the variation of the heat capacity and the fluctuations of the overlap of the average structure with the native structure with temperature can provide some information about the correspondence between nativelikeness and energy.

1. Introduction

Predicting protein structure and the simulation of protein folding from first principles is one of the greatest challenges of contemporary computational biology and biophysics.[1] In the case of protein structure prediction, methods that implement direct information from structural databases (e.g., homology modeling and threading) are, to date, more successful compared to physics-based methods; however, only the latter will enable us to extend the application to simulate protein folding and to understand the folding and structure-formation process. The underlying principle of physics-based methods is the thermodynamic hypothesis formulated by Anfinsen,[2] according to which the native structure of a protein corresponds to the global minimum of its free energy under given conditions. Thus, energy-based protein structure prediction is formulated in terms of a search for a conformation corresponding to the global minimum of an appropriate potential-energy function without the use of ancillary information from structural databases.

To address the problem of the physics-based prediction of protein structure, we have been developing a physics-based united-residue force field, hereafter referred to as UNRES,[3−11] for off-lattice protein-structure simulation. Reduction of the complexity of the problem (i.e., the number of interaction sites and variables) with UNRES is necessary to carry out simulations in real time. However, in contrast to most united-residue force fields that are largely knowledge-based potentials, UNRES was carefully derived on the basis of the physics of interactions.

* Corresponding author. E-mail: has5@cornell.edu. Phone: (607) 255-4034. Fax: (607) 254-4700.
† Cornell University.
‡ University of Gdańsk.

10.1021/jp040327c CCC: $27.50
Published on Web 10/02/2004

We have also developed a very efficient genetic-type algorithm, the conformational space annealing (CSA) method,[12,13] to locate the global minimum.

The condition that the native structure have the lowest energy is necessary but not sufficient both when considering the real folding process and when designing an energy function for folding simulations because it does not guarantee that the lowest-energy structure will be located by a random search, which largely simulates the process of spontaneous protein folding in real systems. This observation was the basis of the so-called paradox formulated by Levinthal,[14] who remarked that the time to locate the native structure by a purely random search for a 100-residue protein would be comparable to the age of the universe even when assuming that each amino acid residue has only two conformational states and that conformational transitions occur on a femtosecond time scale. On the basis of spin-glass theory and the associative-Hamiltonian model, Wolynes and co-workers found that searchable potential functions must maximize the ratio of the folding temperature to the glass-transition temperature (T_f/T_g);[15] this is the principle of minimal frustration. The ratio T_f/T_g is closely related to the quantity widely used in statistics and is called the Z score (Z). In the case of potential-function optimization, the Z score is defined as the difference between the mean energy of the nativelike structures and the mean energy of the non-native structures divided by the standard deviation of the energy of the non-native structures, as given by eq 1[6,9,15−23]

$$Z = \frac{(1/N_{\mathrm{nat}})\sum_{i=1}^{N_{\mathrm{nat}}} E_i - (1/N_{\mathrm{non-nat}})\sum_{i=1}^{N_{\mathrm{non-nat}}} E_i}{\sqrt{(1/N_{\mathrm{non-nat}})\sum_{i=1}^{N_{\mathrm{non-nat}}} E_i^2 - [(1/N_{\mathrm{non-nat}})\sum_{i=1}^{N_{\mathrm{non-nat}}} E_i]^2}} \quad (1)$$

where nat and non-nat indicate the sets of nativelike and non-native conformations, respectively.

Subsequently, on the basis of simulation studies of a model lattice protein, Shakhnovich and co-workers[24] suggested that the sufficient condition for foldability is the presence of a sufficiently large energy gap between the native structure and the lowest-energy non-native structure (eq 2). According to these workers,[24] a large energy gap (also referred to as the standard energy gap; the numerator in eq 1 is referred to as the stability gap[21−23,25]) will provide a driving force to conduct the system to the global energy minimum.

$$\Delta E = \min_{i\in\mathrm{nat}} E_i - \min_{i\in\text{non-nat}} E_i \quad (2)$$

Equations 2 and 1 provide two possible choices of a target function for potential optimization, namely, ΔE and Z. It should be noted that the idea of using the energy gap (eq 2) as a target function was introduced earlier by Crippen and co-workers,[26,27] although the purpose of their approach was to distinguish the nativelike structure from non-native structures on the basis of energy. Substantial further work on optimizing potential-energy functions, based on the minimization of ΔE, Z, or both (or, equivalently, maximization of $-\Delta E$, $-Z$, or both), has been carried out[6,9,15−23,28−31] with energy functions for both threading and de novo folding. This approach was also used in our work[9,20] to optimize the UNRES force field.[3−6,8−11] Hao and Scheraga[19] found that the use of either of the two target functions yields comparable results. Recently, by using the cumulant expansion of the free energy, Wolynes and co-workers demonstrated that the optimizations of ΔE, Z, and the free-energy gap between the native and the unfolded state are equivalent provided that T_g is used as the unit of energy.[22]

Optimizing a single energy gap and Z score alone is, however, not sufficient. The resulting energy landscape can be compared to a weakly diversified terrain with a deep tectonic lake; once the region with the lake is located, it is easy to find the deepest point, but it is not so easy to locate this region. Rather, the energy landscapes should be comparable to caldera-like terrains, where the energy level is gradually lowered when approaching the lowest point.[23] Attempts to optimize potential-energy functions were recently made by the Wolynes group;[22,23] they defined a continuous variable Q, measuring the nativelikeness, and required that the energy be lowered with increasing Q. A procedure that weighted the target energy gap of a conformation with respect to the energy of the experimental structure depending on the rmsd from the native structure was described earlier by Maiorov and Crippen.[32] Recently, Micheletti and co-workers[29] and Fain and Levitt[31] proposed methods in which the target function is a sum of energy gaps between nativelike and non-native conformations weighted by their rmsd.

In our recent work,[11] we proposed a novel approach to optimize energy functions to obtain caldera-like landscapes. The method assumes a hierarchical structure of the energy landscape, which means that the energy decreases as the number of nativelike elements in a structure increases, being lowest for structures from the native family and highest for structures with no nativelike element. Preliminary applications to the designed peptide 1FSD (a minimal 28-residue $\alpha + \beta$ motif)[11] and the third IgG-binding domain from streptococcal protein G (a 61-residue $\alpha + \beta$-protein referred to in the PDB as 1IGD[33])[11,34] showed that the method performs much better than the classical energy gap and Z-score optimization approach. (The latter failed for 1IGD). In this paper, we report the assessment of the approach using simple lattice protein models for which all conformations can be enumerated. We demonstrate that an appropriate design of the hierarchy of structure formation is critical to the success of the method. The two accompanying papers[35,36] are devoted to the use of the method to optimize the UNRES off-lattice potential energy function on a single[35] and on many[35] proteins.

2. Methods

2.1. Lattice Model of the Polypeptide Chain and Potential-Energy Function. As in our previous work on force-field optimization,[20] we used a simple cubic-lattice model of polypeptide chains to provide initial tests of the method.

Each chain is a self-avoiding walk on the lattice, the nodes corresponding to the positions of the C^α atoms of amino acid residues. A chain contains two types of interaction sites: side chains and peptide groups. The positions of side-chain centers coincide with those of the C^α atoms, whereas the peptide groups are placed in the middle between the consecutive C^α atoms. The side chains are the centers of hydrophobic/hydrophilic interactions; consequently, two types of side chains (and also amino acid residues) are distinguished—hydrophobic (H) and polar (P)—which implies three different values of the contact energy between the side chains (eq 3). It should be noted that although we use the symbols H and P to denote the types of residues our model is not equivalent to the HP model of Dill and co-workers[37] because of the presence of peptide groups and also local interaction terms in the potential (eq 3). The peptide groups are the centers of backbone−hydrogen-bonding (electro-

TABLE 1: Values of the Torsional Energy (kcal/mol) for All Pairs of Residue Types[a] and the Values of Virtual-Bond Dihedral Angles Allowed for the Cubic-Lattice Model[8]

	−90°	0°	+90°	+180°
Ala-Ala	0.74	1.15	0.49	0.00
Ala-Gly	0.30	0.16	0.20	0.00
Ala-Pro	0.28	6.34	0.72	0.00
Gly-Ala	0.45	0.12	0.10	0.00
Gly-Gly	0.27	0.34	0.27	0.00
Gly-Pro	0.70	0.83	0.17	0.00
Pro-Ala	0.97	0.70	0.19	0.00
Pro-Gly	0.57	0.27	0.02	0.00
Pro-Pro	0.12	19.90	−0.62	0.00

[a] The values at +90 and −90 for the Ala- and Pro-type residues differ because these residues are chiral; therefore, their ECEPP-based virtual-bond torsional potentials are not symmetrical.

static) interactions. The energy of the lattice chain is expressed by eq 3.

$$V = \epsilon_{HH}N_{HH} + \epsilon_{HP}N_{HP} + \epsilon_{PP}N_{PP} + \epsilon_{el}N_{el} + e_{bend}N_{bend} + w_{tor}\sum_{k=1}^{N_{tor}} U_{tor}(\gamma_k) \quad (3)$$

where N_{XY} and ϵ_{XY} are the number of contacts and the contact energy between nodes of type X and Y, respectively, N_{el} and ϵ_{el} are the number of contacts and the contact energy, respectively, of the peptide groups, N_{bend} is the number of consecutive virtual bonds at the 90° angle, e_{bend} is the energy of the change in a virtual-bond angle from 180 to 90°, N_{tor} is the number of virtual-bond dihedral angles in the lattice chain, γ_k is the value of the kth dihedral angle (the only values possible on a cubic lattice are 0, 180, and ±90°), and w_{tor} is the weight of the torsional energy U_{tor}. A contact between two peptide groups corresponds to the formation of a backbone hydrogen bond. A contact between two peptide groups occurs when they are separated by exactly one lattice unit. Consequently, the corresponding virtual bonds are separated by exactly one lattice unit and are either parallel or antiparallel. These configurations are close to the configurations of hydrogen-bonded peptide groups in β-sheets or α-helices. It should be noted that, in contrast to the UNRES energy function,[3−11] only one energy-term weight (w_{tor}) appears here. This is because the first three terms in eq 3 correspond to the side-chain interaction potential ($U_{SC_iSC_j}$), which has a weight of 1 in UNRES. The fourth and the fifth terms correspond to the peptide-group interaction ($U_{p_ip_j}$) and the bending potential (U_b) of UNRES, respectively; because these potentials become highly simplified in the cubic-lattice representation, their weights are absorbed into the parameters ϵ_{el} and e_b, respectively.

As in UNRES, three types of amino acid residues were considered to determine the torsional energy: glycine (Gly), proline (Pro), and alanine (Ala), the latter representing all residues except Gly and Pro. The torsional potentials were a discretized version of the ECEPP-based virtual-bond torsional potentials determined in ref 8; the values of the torsional energies[8] are summarized in Table 1.

We considered 12-residue lattice chains. This system is small enough to take into account all possible conformations (a total of 1 747 257) while optimizing the energy function (see Results), and at the same time, the chain is long enough to produce nontrivial structures. This enabled us to enumerate all of the conformations by using the backtrack algorithm, as in our earlier work.[20] Tests of foldability were carried out by means of the canonical Metropolis Monte Carlo algorithm, the moves being end moves, spike moves, and crankshaft moves.[38] These moves are illustrated in Figure 1.

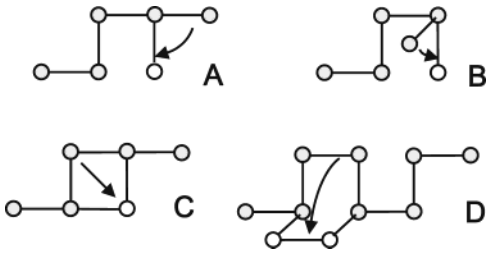

Figure 1. Illustration of bead moves on the cubic lattice: end moves (A and B), the spike move (C), and the crankshaft move (D).

2.2. Hierarchical Optimization Algorithm. Here we describe the simplified version of the optimization algorithm adopted from our earlier paper,[11] which was applied to on-lattice models with enumerable conformational space. Because its recent development pertains to the UNRES potential-energy function and an off-lattice chain, we leave the description of the off-lattice version to the first of the accompanying papers.[35]

1. Determine all distinct self-avoiding conformations of the model. As in our previous work,[20] we use the backtrack algorithm.[39]

2. Define the elementary fragments of the molecule. For on-lattice models, the fragments are defined in terms of native contacts.

3. Define the hierarchy levels of the protein in terms of elementary fragments.

4. Minimize the target function Φ defined by eq 4.

$$\Phi = \sum_{i=1}^{n} w_i g[F_i(\beta) - F_{i+1}(\beta); -\infty, -\Delta_i] + \sum_{i=1}^{n} w_i g[Z_i(\beta'); -\infty, -\zeta_i] \quad (4)$$

with

$$g(x; x_{min}, x_{max}) = \begin{cases} {}^1/_4(x - x_{min})^4 & x < x_{min} \\ {}^1/_4(x - x_{max})^4 & x > x_{max} \\ 0 & \text{otherwise} \end{cases} \quad (5)$$

and the w's being the weights of the respective terms in the target function. F_i is the configurational free energy of level i (defined by eq 6), Z_i is the Z score computed between levels i and $i + 1$ (defined by eq 7), Δ_i and ζ_i are the minimum required free-energy and Z-score gaps between levels i and $i + 1$, and β and β' are the inverses of the reduced temperatures at which the free energies and Z scores, respectively, are computed. If $\Phi = 0$, then none of the gaps are greater than the required minimal values; otherwise, some of the minimal gaps are not achieved.

$$F_i(\beta) = -\frac{1}{\beta}\ln\sum_{k\in\{i\}}\exp(-\beta E_k) \quad (6)$$

$$Z_i(\beta') = \frac{\langle E_{\{i+1\}}\rangle_{\beta'} - \langle E_{\{i\}}\rangle_{\beta'}}{\sqrt{\langle E^2_{\{i\}}\rangle_{\beta'} - \langle E_{\{i\}}\rangle^2_{\beta'}}} \quad (7)$$

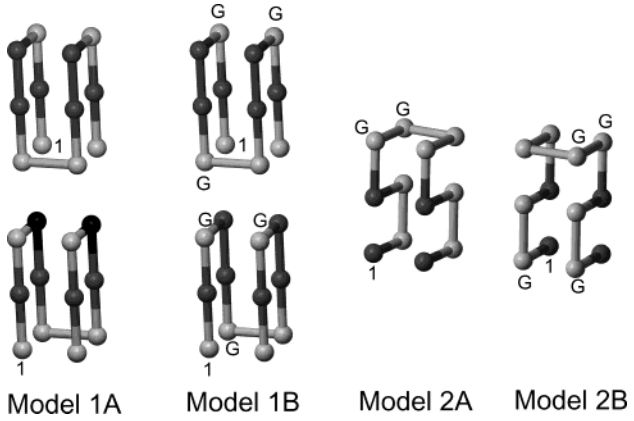

Figure 2. Native structures of the four 12-bead lattice peptide chains of models 1A and 1B and models 2A and 2B. The first residues are marked with a "1", the hydrophobic residues are shown as dark spheres, the polar residues are shown as light spheres, and the glycine residues are marked with a "G". Models 1A and 1B have a doubly-degenerate native structure, with two mirror images being shown. Model 1B differs from model 1A by the placement of glycine residues at turn positions.

where $\{i\}$ denotes the set of structures belonging to level i and $\langle A\rangle_\beta$ denotes the canonical average of quantity A at inverse temperature β:

$$\langle A\rangle_\beta = \frac{\sum_k A_k \exp(-\beta E_k)}{\sum_k \exp(-\beta E_k)} \tag{8}$$

In this paper, we set $\beta = 10$ and $\beta' = 0$, which means that the free energy of a level is effectively the energy of its lowest-energy conformation and the Z score is computed using regular and not canonical averages. We chose these settings for the sake of compatibility with the definitions of the energy gap and Z score given by eqs 1 and 2. Nonhierarchical optimization was also carried out by minimizing Φ; in this case, the set of conformations was divided into only two levels, the first one consisting of all structures except native and the second consisting of the native structure (or structures in the case of degenerate native levels).

2.3. Procedures and System Studied. To study the behavior of the hierarchical algorithm, we chose four models, hereafter referred to as model 1A, model 1B, model 2A, and model 2B, respectively. Each of the four models is defined by a given sequence and a given native structure. The sequences were the following: PHPHHPPHHPHP for model 1A, PHGHHGPHH-GHP for model 1B, HPPHGGPPHPPH for model 2A, and HGPHPPGGHPGH for model 2B. Here, H and P denote a hydrophobic and a polar residue, respectively, with an alanine-like pattern of local interactions, and G denotes a glycine residue, which is considered to be polar. These sequences and the corresponding native structures are shown in Figure 2. The native structures shown in Figure 2 were chosen to correspond to protein-like topologies (β and α, respectively); the glycine residues are in the positions of turns in the native structures as usually occurs in proteins. We chose protein-like models rather than models with native structures, defined as any accidental compact structures of a 12-residue cubic-lattice chain, because our potential-function optimization method is designed for protein energy landscapes (or, generally, for the energy landscapes of polymers with a significant content of regular secondary structure) and not for the energy landscapes of arbitrary polymers. The native structures of models 1A and 1B are identical, and these models differ only by sequence. The native structures of models 2A and 2B are mirror images of each other, and their sequences also differ. Below we provide a short description of the four models.

We shall denote the lattice structures by sequences of consecutive virtual-bond vectors (from 1 to $n - 1$, with n being the number of beads) that are defined as follows: $\mathbf{0} = [1, 0, 0]$; $\mathbf{1} = [0, 1, 0]$; $\mathbf{2} = [0, 0, 1]$; $\mathbf{3} = [-1, 0, 0]$; $\mathbf{4} = [0, -1, 0]$; $\mathbf{5} = [0, 0, -1]$. The integers in each triad denote the xth, the yth, and the zth coordinates, respectively, the unit of measure being the lattice unit. These six vectors define the only directions in which a virtual bond can point on a cubic lattice provided that the elementary cell is aligned with the Cartesian coordinate system. To provide a unique structure definition, the first vector is **0**, and the first vector after the chain starts to bend (usually this is the second vector) is **1**. For example, the sequences **00000000000** and **01010101010** denote a completely extended and a "zigzag" 12-bead chain, respectively.

Models 1A and 1B have the same native structure, which is a minimal β-barrel (Figure 2). The native structure is doubly degenerate (the two structures being mirror images defined by sequences of virtual-bond vectors **00133200433** and **00133500433**, respectively) with the potential given by eq 3 because the virtual-bond dihedral angles are undefined in the turn regions and there is, therefore, no energy term to differentiate the two mirror images. Simulations for this model are, therefore, similar to those of Shakhnovich and co-workers[24,40] because these authors used only a contact potential that also does not distinguish mirror images. The native structures of models 1A and 1B are stabilized by five hydrophobic contacts between residues 2 and 5, 2 and 11, 4 and 9, 5 and 8, and 8 and 11.

The native structure of model 2A is defined by the sequence of virtual-bond vectors **01310234043**, and that of model 2B is defined by **01310534043**. (As mentioned earlier in this section, the native structures of models 2A and 2B are mirror images of each other.) These structures consist of two sequences of turns packed antiparallel to each other; therefore, to some extent, they can be regarded as a model of the helix-turn-helix motif (Figure 2). For each of these two models, the native structure is unique because its mirror image (**01310534043** for model 2A and **01310234043** for model 2B) is differentiated from it by the torsional potential (i.e., the difference in the torsional energy at $\gamma = 90°$ and $\gamma = -90°$, respectively; see Table 1). For both models 2A and 2B, the native structure is stabilized by four hydrophobic contacts between residues 1 and 3, 1 and 12, 3 and 9, and 9 and 12 (Figure 2).

For each system, we produced several sets of energy parameters, which differed by the optimization scheme (hierarchical or not, type of hierarchy for hierarchical optimization, and the target energy and Z-score gaps, respectively). For each optimization scheme, we started the minimization of the target functions from 20 random sets of parameters of the energy function (eq 3); these usually led to several distinct sets of parameters but sometimes converged to a unique solution. Each optimization was carried out using the whole set of enumerated conformations.

To test all potentials, for each system and each set of energy parameters, 20 canonical 20 000-step MC simulations were carried out at reduced temperatures selected to capture the quickest folding and the maximum number of hits of the native structure. Thus, the number of steps was smaller by 2 orders of magnitude than the total number of conformations of a 12-bead chain on a cubic lattice; therefore, it is not likely to find the native structure by a purely random search with any energy

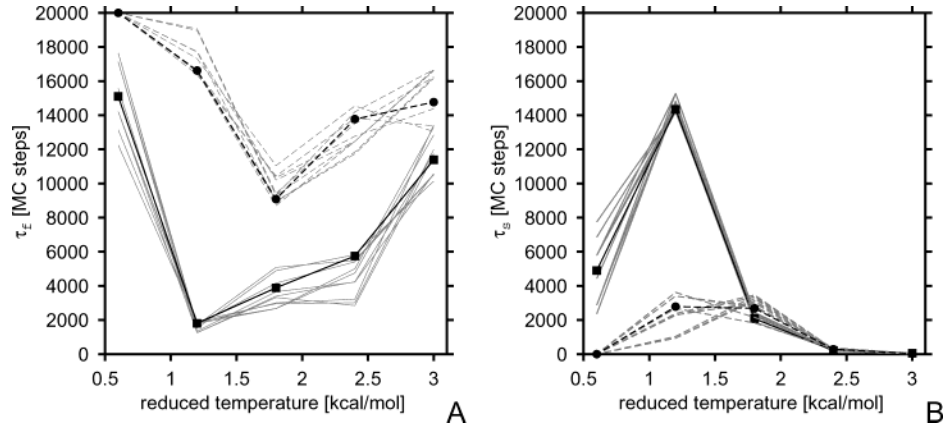

Figure 3. Dependence of τ_f (A) and τ_s (B) on reduced temperature for a sample good folder (solid lines and filled squares) and for a sample bad folder of model 1A (dashed lines and filled circles) obtained in nonhierarchical optimization. The thick black lines with symbols represent the curves obtained after averaging the data from 20 MC runs, and the thin gray lines (solid and dashed) represent the curves obtained after averaging from runs 1−10, 2−11, ..., 11−20.

parameters. The reduced temperatures ranged from 0.4 to 7.0 kcal/mol, and typically, runs at 5−8 temperatures were carried out. The number of MC steps (20 000) was chosen empirically because the average number of steps to find the native structure was about 1000 for the best and about 10 000 for average folders. To assess the foldability of a particular system at reduced temperature (θ), we used two types of measures: the average number of MC steps to find the native structure or the folding time ($\tau_f(\theta)$, also referred to as the mean first passage time (MFPT)[25]) and the average number of steps spent in the native structure or the stability time ($\tau_s(\theta)$); they measure the fastness of folding and the stability of the respective native structure, respectively. The definition of $\tau_s(\theta)$ is self-explanatory; to define $\tau_f(\theta)$ we used the following equation:

$$\tau_f(\theta) = \frac{1}{20}\sum_{i=1}^{20} \tau_f^i \tag{9}$$

$$\tau_f^i = \begin{cases} \text{MC step at which the native structure was found} \\ \quad \text{in simulation } i \\ 20\,000 \text{ if the native structure was not found} \\ \quad \text{in simulation } i \end{cases} \tag{10}$$

The global characteristics of folding were τ_f^{min} and τ_s^{max} defined by eqs 11 and 12, respectively:

$$\tau_f^{min} = \min_{\theta} \tau_f(\theta) \tag{11}$$

$$\tau_s^{max} = \max_{\theta} \tau_s(\theta) \tag{12}$$

For further analysis, we also define the reduced temperatures $\theta(\tau_f^{min})$ and $\theta(\tau_s^{max})$ corresponding to the miminum folding time and maximum content of the native structure, respectively, as well as the folding time at the reduced temperature with the maximum stability of the native structure $\{\tau_f(\tau_s^{max}) \equiv \tau_f[\theta(\tau_s^{max})]\}$ and the stability time at the reduced temperature corresponding to the minimum folding time $\{\tau_s(\tau_f^{min}) \equiv \tau_s[\theta(\tau_f^{min})]\}$.

Sample $\tau_f(\theta)$ and $\tau_s(\theta)$ curves for a good and a bad folder, respectively, corresponding to averages over half of the data (10 MC runs) and the complete data set (20 MC runs), respectively, are shown in Figure 3. It can be seen from the differences between the averages over parts of the data sets (10 MC runs; thin gray lines) and the complete data sets (thick darker lines) that the accuracy of the determination of these quantities is less than 1000 MC steps for a good and about 2000 MC steps for a bad folder; this is sufficient to distinguish the folders on a semiquantitative basis. We also performed trial calculations with a greater number of trajectories (50 and 100) and a greater variation of the number of MC steps in a single run (5000, 10 000, 20 000, 50 000, 100 000, and 200 000) for a sample good, average, and bad folder. The resulting τ_f^{min} values were compared directly, and the τ_s^{max} values corresponding to simulations with a different number of MC steps were scaled to 20 000 MC steps. We found that for good and average folders the estimated accuracy is of the same order as the above estimate when at least 10 000 steps and 10 trajectories are used; for bad folders, at least 20 000 MC steps must be performed in a single simulation. The accuracy did not change remarkably even with the greatest number of MC steps and trajectories. Increasing the accuracy would, therefore, require a considerable increase in computational effort per system studied. Because the systems studied are highly simplified, higher accuracy does not seem to be necessary to study the behavior of various optimization schemes qualitatively; it appeared more important to us to run simulations with a great variety of energy-function parameters.

3. Results and Discussion

3.1. Models 1A and 1B. We start the discussion with models 1A and 1B, which exhibit simpler behavior than models 2A and 2B and for which the results are more directly related to those obtained earlier by Shakhnovich and co-workers.[24,40] The settings of all runs are summarized in Table 2. The value of ϵ_{HH} was fixed at −1.0 kcal/mol to avoid an uncontrolled increase of the total energy. The results of all calculations for models 1A and 1B are summarized in Table 3.

Nonhierarchical Optimization with Model 1A. The first set of calculations was carried out on model 1A in a nonhierarchical mode (i.e., setting a single free-energy and *Z*-score gap between the native structures and the remaining structures, irrespective of the possible content of native elements in the latter). We carried out three such runs, which differed by the minimal free-energy and *Z*-score gaps imposed (Table 2).

In the first round of optimization runs, a small target energy gap of 3 kcal/mol was imposed (Table 2). We used 40 random starting sets of parameters of the potential-energy function, all of which resulted in different final parameters. For most of these sets, only the minimum target free-energy gaps were reached;

TABLE 2: Values of Target Energy (Δ) and *Z*-Score (ζ) Gaps and the Ranges of Initial Parameters[a] for Models 1A and 1B

model	hierarchy[b]	set[c]	Δ[d] (kcal/mol) 0−1	1−2	2−3	3−4	ζ[d] 0−1	1−2	2−3	3−4
1A	none	1	3.0				2.0			
		2	8.0				2.0			
		3	20.0				2.0			
1A	box_{112}[e]	1	10.0	10.0			3.0	2.0		
1A	box_{222}[e]	1	10.0	10.0			3.0	2.0		
1A	M1H1	1	2.0	2.0	2.0		1.5	1.5	1.5	
1A	M1H2	1	2.0	2.0	2.0		1.5	1.5	1.5	
1A	M1H3	1	2.0	2.0	2.0	2.0	1.5	1.5	1.5	1.5
		2	5.0	1.0	1.0	1.0	2.0	1.5	1.5	2.0
		3	2.0	1.0	5.0	10.0	1.5	1.0	2.0	3.0
		4	8.0	1.0	2.0	10.0	2.0	1.0	1.5	3.0
		5	8.0	5.5	2.5	1.0	2.0	2.0	1.0	1.0
1A	M1H1r	1	8.0	2.0	2.0		1.5	1.5	1.5	
		2	10.0	1.0	1.0		1.5	1.5	1.5	
1B	none	1	3.0				2.0			
		2	8.0				1.0			
		3	10.0				3.0			
1B	M1H3	1	2.0	2.0	2.0	2.0	1.0	1.0	1.0	1.0
		2	8.0	2.0	2.0	10.0	1.0	1.0	1.0	2.0

[a] The initial values of ϵ_{HP}, ϵ_{PP}, ϵ_{el}, ϵ_{bend}, and w_{tor} are in the range of [−5...5]. [b] See the text and Figure 5 for the description of hierarchies. [c] Denotes the number of the set of calculations for a given system (model and hierarchy) but different target energy and *Z*-score gaps. [d] Target energy and *Z*-score gaps (eq 4) between consecutive levels marked as $i - j$ for a gap between levels i and j, the highest level being the native level. For nonhierarchical optimizations, level 0 denotes all structures except native and level 1, the native structure. [e] Nonhierarchical optimization with additionally setting an energy and *Z*-score gap between the structure confined to a $1 \times 1 \times 2$ or a $2 \times 2 \times 2$ box, respectively, and noncompact structures.

however, larger gaps were obtained for a few of them. To provide more data for larger energy gaps, we carried out another round of 20 optimizations and subsequent MC simulations assuming an energy gap of 8 kcal/mol. This resulted in 20 sets of distinct parameters. Finally, we carried out one round of optimizations with the target energy gap of 20 kcal/mol; an energy gap of 14.3 kcal/mol was achieved given the limits imposed on the energy parameters.

With the optimized parameters of the potential-energy function (a total of 80 sets), we ran MC simulations to determine the respective folding times (τ_f^{min}) and the stability of the native structure (τ_s^{max}); these quantities are plotted in Figure 4 as functions of energy and *Z*-score gaps. Here we observe a general pattern: with increasing $-\Delta E$, the smallest τ_s^{max} increases, and the highest τ_f^{min} decreases. In other words, increasing the target energy gap makes it more probable to obtain a good folder, as found earlier by Shakhnovich and coworkers.[24,40] However, excellent folders are also obtained with smaller energy gaps; therefore, a large energy gap does not seem to be a necessary condition for a good folder. In particular, both very poor (with $\tau_s^{max} \approx 1500$) and excellent (with $\tau_s^{max} \approx 18\,000$) folders are encountered among systems with about a 3 kcal/mol gap.

It should be noted that the energy gap was defined by Shakhnovich and co-workers[40] as the gap between the native structure (which was maximally compact) and the next maximally compact structure; this energy gap is referred to as the compact energy gap.[25] Shakhnovich subsequently argued that this is just the proper definition of an energy gap because structures differing just by a flip of a bead would presumably have a similar energy to that of the native structure but would not be different enough.[41] We therefore examined the sets of low-energy non-native structures and found that they are usually either next to the native structures in energy or the energy difference between the lowest-energy non-native and the lowest-energy non-native maximally compact structure is small. Nevertheless, τ_s^{max} and τ_f^{min} are plotted as functions of the energy gaps ($-\Delta E_c$) between the native structures and the lowest-energy maximally compact non-native structures in Figure 4E and F. It can be seen that there is still no tight correlation between the redefined energy gap and these quantities. This shows that the compact energy gap is not a good determinant of foldability. To provide a final proof that compactness and a large energy gap do not guarantee good folders, we carried out two series of optimizations in which an energy gap of 10 kcal/mol was imposed between structures confined to boxes of dimensions $1 \times 1 \times 2$ and $2 \times 2 \times 2$ lattice units, respectively, and noncompact structures; these settings are referred to as box_{112} and box_{222}, respectively. It can be seen (Table 3) that forcing maximum compactness (box_{112}) impairs foldability and with less compactness (box_{222}) the results are comparable to those obtained with no constraints.

It must be pointed out that the absolute energy gap might not be a good measure of the energy difference between the native state and non-native states because it does not contain information about the spread of the energy. However, the *Z* score, which is the energy difference scaled by the standard deviation of the energy of non-native structures, shows an even worse correlation with foldability measures (compare Figure 4C to A and Figure 4D to B). Therefore, the results of the simulations reported here suggest that other factors, such as the structure of the energy levels, as suggested in our previous work,[11] rather than the energy gap or *Z* score may be the main determinants of foldability.

We also tried to correlate τ_f^{min} and τ_s^{max} with the σ parameter (eq 13 in section 3.3) introduced by Thirumalai and coworkers.[25,42−44] We did not find clear correlations for the system studied. However, there seems to be some relationship between the structure of the energy spectrum and the structure of the curves for the temperature dependence of the heat capacity of the system ($C_v(T)$; eq 14 in section 3.3) and the average overlap with the native structure curves ($\chi(T)$; eq 15 in section 3.3). We address this issue for all models studied in section 3.3.

To determine whether the energy levels are ranked according to the content of native-structure elements, we analyzed the energy levels in terms of the content of structural organization. Level 0 was defined as a set of structures with no native β-hairpin; level 1, a set of structures with one hairpin; and level 2, a set of structures with at least two hairpins. Level 3 contained only the native structures. The hairpins were defined in terms of contacts, as given in Figure 5, and this structural hierarchy is hereafter referred to as hierarchy M1H1 (hierarchy 1 of model 1). In Figure 6, we analyze selected energy spectra corresponding to good, average, and bad folders resulting from nonhierarchical optimization in terms of the assignment of the structures to levels of hierarchy M1H1. It can be seen that the energy spectra of particularly bad folders (i.e., with the lowest τ_s^{max} and the largest τ_f^{min} values) exhibit a high density of low-energy states with no elements of the native structure whereas the states belonging to level 2 are high in energy (Figure 6D). This supports the principle of the hierarchical-optimization algorithm: if the ordering of energy levels is very important for the foldabilty of a 12-residue chain treated at a very simplified level, then it can be anticipated to be absolutely

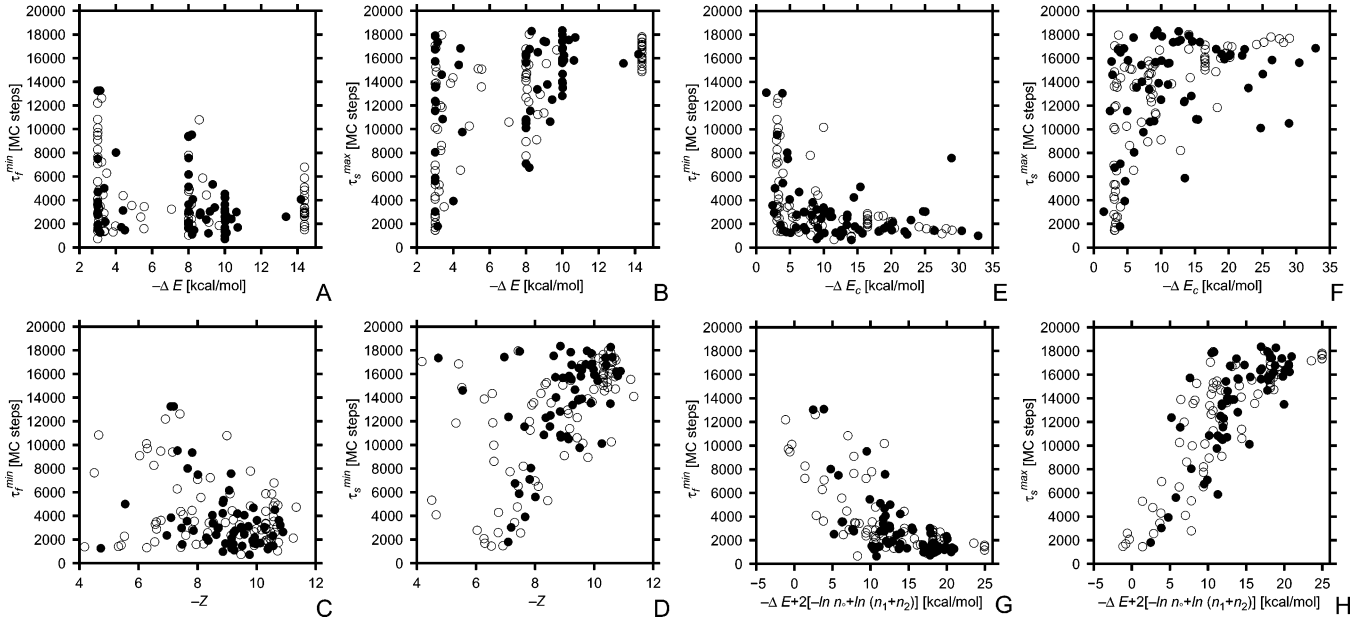

Figure 4. Scatter plots of the relationship of τ_f^{min} (A) and τ_s^{max} (B) with the standard energy gap (ΔE), τ_f^{min} (C) and τ_s^{max} (D) with the Z score, τ_f^{min} (E) and τ_s^{max} (F) with the compact energy gap (ΔE_c; defined as the energy difference between the native structure and the lowest-energy maximally compact structure), and τ_f^{min} (G) and τ_s^{max} (H) with the sum of the energy gap and the difference between the logarithms of the occupation of levels with and without native elements ($\Delta E - 2[\ln(n_1 + n_2) - \ln n_o]$) for nonhierarchical optimizations of model 1A (filled circles) and 1B (empty circles).

essential for a polypeptide chain of a real size (50 amino acid residues and more), for which the fraction of the number of conformations that can be visited in real time to the total number of conformations (or, generalizing to off-lattice models, the fraction of searchable conformational space) is smaller than it is here by several tens of orders of magnitude.

However, it can also be seen from Figure 6B that although the proper ordering of energy levels results in a fast folder (small τ_f^{min}) it does not guarantee the stability of the native structure. It can be seen that large τ_s^{max} values are obtained for those systems for which the density of the energy levels of low-energy structures with nativelike elements is high (or, in other words, the average energy-level separation is small) compared to the energy gap between the native and the lowest-energy non-native structure (Figure 6A). This can easily be explained in terms of the arguments put forward by Wolynes and co-workers:[22] if the energy gaps between near-native structures (which are related to the barrier separating the native structure from non-native structures and, therefore, to the folding temperature) are comparable to that between the native and lowest-energy non-native structure, the average energy barrier to overcome in the last stage of folding will be comparable to the energy gain in the formation of the native structure. Therefore, at temperatures approaching the folding temperature (Figure 6B), the system will frequently escape from the native structure, once it is found, and, consequently, the native structure will not have sufficient thermodynamic stability.

The above observations are illustrated even better in Figure 4G and H, in which τ_s^{max} and τ_f^{min} are plotted as functions of a sum of the energy gap and the difference between the logarithms of the number of states (the entropy) with nativelike elements and those without nativelike elements lying within the energy-gap window. It can be seen that the correlation is very good for τ_s^{max} and still reasonable for τ_f^{min}. A similar relationship between the entropy of non-native states and folding time or the difference in the free energy of the folded and unfolded states and the folding time was observed by Klimov and Thirumalai.[25,43]

An analysis of the energy spectra also reveals that when the energy gap between the native and non-native structures increases gradually fewer structures with no nativelike elements appear in the low-energy part of the spectrum. This is illustrated in Figure 7, in which the logarithm of the number of structures with at least one native hairpin within an energy window equal to the energy gap is plotted as a function of the energy gap. This means that increasing the target energy gap induces some ordering of the energy levels. It must be noted, however, that typical free-energy gaps are on the order of 3 kcal/mol for β-proteins, 7 kcal/mol for α/β-proteins, and 8−10 kcal/mol for α-proteins. (See, for example, Table 1 in ref 45.) Therefore, forcing an arbitrarily large energy gap seems to have little relevance to the physics of folding.

Hierarchical Optimization with Model 1A. Next, we carried out hierarchical optimizations of model 1A assuming hierarchy M1H1, as in the above analysis of the results of nonhierarchical optimizations. A small target energy gap was set between the native structures and the next level (Table 2), and all optimizations led to reaching or exceeding the target gaps. The plots of τ_s^{max} and τ_f^{min} as functions of the energy gap are presented in Figure 8. It can be seen that the energy gap is now well correlated with τ_s^{max} (empty squares in Figure 8), the smallest τ_s^{max} (5477 MC steps) being larger than that for nonhierarchical optimization (1457 MC steps). Moreover, the largest τ_f^{min} is only 3215 MC steps, which means that folding is kinetically facilitated. This supports the conclusion drawn from the results of nonhierarchical optimizations that ensuring proper energy ordering of structural levels results in fast folders and additionally providing a large enough energy gap between the native and lowest-energy non-native structures ensures the stability of the native state. The correlation between $-\Delta E$ and τ_s^{max} occurs because we set the same energy gaps between levels in all hierarchical optimizations with model 1A and, consequently,

TABLE 3: Summary of the Results of Monte Carlo Simulations with Optimized Potential-Function Parameters for Models 1A and 1B

model[a]	hierarchy[a]	set[a]	NP[b]	$\theta(\tau_s^{max})$[c]	$\tau_f(\tau_s^{max})$[c]	τ_s^{max} [c]	$\theta(\tau_f^{min})$[c]	τ_f^{min} [c]	$\tau_s(\tau_f^{min})$[c]
				1.80	2571	15 109	1.20	1592	13 566
		1	40	1.80	15 334	1685	2.40	10 828	925
				1.68	8053	8867	1.77	4550	5226
				1.20	1899	18 017	1.80	897	17 128
1A	none	2	20	1.80	9395	7734	3.00	10 166	6371
				1.89	4700	13 715	2.16	3238	10 442
				2.40	1457	17 803	2.40	1159	17 640
		3	20	2.40	2640	14 866	2.40	2859	15 949
				2.13	2242	16 501	2.67	2013	14 281
				3.00	3498	13 870	3.00	3423	13 588
1A	box_{112}	1	20	2.40	12 102	7594	2.40	10 856	8788
				2.97	6620	11 631	2.97	6128	11 237
				1.80	1911	16 581	2.40	733	8795
1A	box_{222}	1	20	2.40	11 803	7169	3.50	7702	3592
				2.63	5160	12 404	2.89	3908	8411
				1.80	727	17 845	2.40	689	13 745
1A	M1H1	1	20	1.20	11 158	5477	1.80	3215	2824
				1.80	4475	12 830	2.25	1710	8035
				1.80	1672	17 500	1.80	1672	17 500
1A	M1H2	1	20	1.20	11 062	2440	1.20	14 316	1045
				1.65	6001	10 712	1.86	4968	6732
		1	1	0.60	1205	13 612	0.60	1205	13 612
		2	1	1.20	1368	16 489	1.80	931	10 221
		3	1	0.60	7788	8866	1.80	981	2090
1A	M1H3			1.20	1732	17 808	1.80	1025	16 084
		4	2	1.20	8687	10 773	2.40	2202	3871
				1.50	5210	14 291	2.10	1613	9978
		5	1	1.20	1748	18 018	1.80	818	16 673
				1.80	11 720	3632	2.40	6220	104
1A	M1H1r	1	19	0.60	9983	12	1.80	18 793	115
				1.55	15 675	956	1.67	13 992	451
		2	1	3.00	15 055	2310	3.00	15 103	2485
				0.60	1594	17 910	1.20	642	7072
		1	20	2.40	13 034	1788	2.40	13 083	63
				1.20	5941	11 551	1.38	3937	7814
				1.20	1460	18 274	1.80	1100	14 830
1B	none	2	20	3.00	9518	6748	3.00	9518	6748
				2.07	4745	13 431	2.31	3228	10 793
				1.80	976	18 352	1.80	715	17 954
		3	20	1.80	5938	12 817	3.00	4224	3247
				1.95	2643	15 898	2.31	1924	12 932
				0.60	997	18 837	1.20	601	6335
1B	M1H3	1	20	0.60	8807	9707	1.20	1169	2736
				0.72	2050	16 349	1.11	879	9765
		2		1.20	1263	18 598	2.40	534	12 884

[a] See the legend to Table 2 for an explanation. [b] Number of different sets of energy-function parameters obtained in optimization. [c] See eqs 11 and 12 and the text of section 2.3 for definitions of these quantities. If more than one set of parameters was obtained for given settings, the results are presented in three consecutive rows. The upper row contains the best results in terms of τ_s^{max} (columns 5−7) and τ_f^{min} (columns 8−10), the middle row, the worst results in terms of τ_s^{max} and τ_f^{min}, and the third row, the averages over all sets of parameters.

the spread of the energy spectrum was comparable for all of the resulting potentials. In contrast to this, there were no gaps except that between the energy of the native and the lowest-energy non-native structure imposed in nonhierarchical optimization; therefore, even if the energy levels happened to be ordered according to the nativelikeness of the corresponding structures (which results in small τ_f^{min} and, thereby, good kinetic foldability), the resulting spectra could still differ in the spread of the energy in the near-native region, which resulted in a variety of τ_s^{max} values for a given standard energy gap.

The ultimate proof of the vital role of energy-level ordering was provided by two additional series of calculations in which the order of the energy levels was reversed while optimizing the energy function; this is referred to as hierarchy M1H1r. The results are summarized in Table 3 and Figure 8. It can be seen that reversing the levels resulted in the worst folders even when a large energy gap was achieved between the native structure and the lowest-energy non-native structure.

The central hairpin of model 1A is stabilized by two hydrophobic contacts (between residues 4 and 9 and residues 5 and 8), and it can thus be considered to initiate folding. Therefore, we next considered hierarchy M1H2 (Figure 5), in which level 1 contained structures with both the 4−9 and 5−8 contacts developed and level 2 consisted of structures with all hydrophobic contacts between the two halves of the chain formed. (An example of such structures is a long β-hairpin comprising the whole chain.) It can be seen from Figure 8 that this hierarchy results in remarkably larger τ_f^{min} values com-

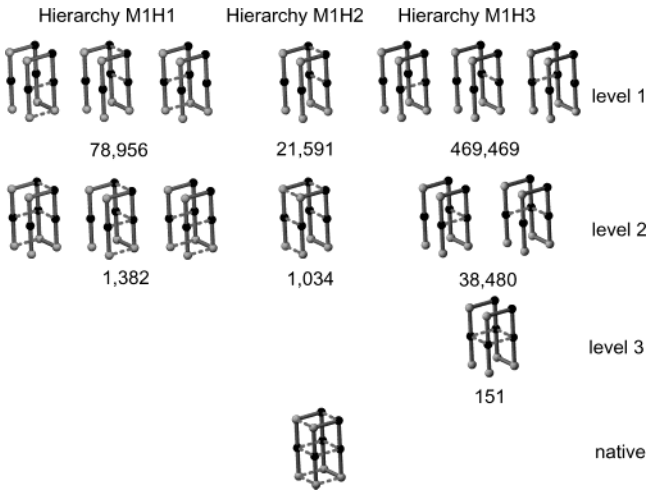

Figure 5. Illustration of the hierarchy levels of models 1A and 1B for hierarchies M1H1, M1H2, and M1H3. The structures classified to given levels are required to possess the native contacts shown in the pictures. Two contacts as in level 1 of hierarchy M1H1 define a hairpin. The contacts are shown as dashed lines on the scaffold of the native structure; a given level must have any one and only one of the contact patterns shown. The number of structures at a given level for a given hierarchy is printed below each level.

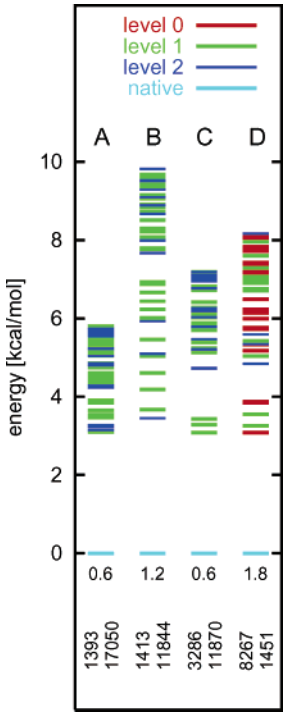

Figure 6. Energy spectra of good and bad folders of model 1A obtained by non-hierarchical optimization. Levels of the 200 lowest-energy structures per column are shown. The values of τ_f^{min} and τ_s^{max}, respectively, are printed for each system on the left and on the right sides below level 0; above them is printed the reduced temperature corresponding to τ_s^{max}. Energy levels are colored according to the number of native hairpins, following hierarchy M1H1 shown in Figure 5. The energy is expressed relative to that of the native structure. (A) Fast and stable folder; the energy levels are ordered according to nativelikeness (this makes a fast folder), and the energy gap is larger than the sparseness of the near-native levels (this makes a stable folder). (B) Fast but less stable folder; the energy levels are ordered according to nativelikeness, but the energy spectrum in the near-native region is sparser than that of folder A, which affects stability. (C) Slower folder, for which the order of levels 1 and 2 is reversed, which affects the speed of folding. (D) Slow folder with low stability of the native structures; the ordering of energy levels next to the native structure is opposite to nativelikeness.

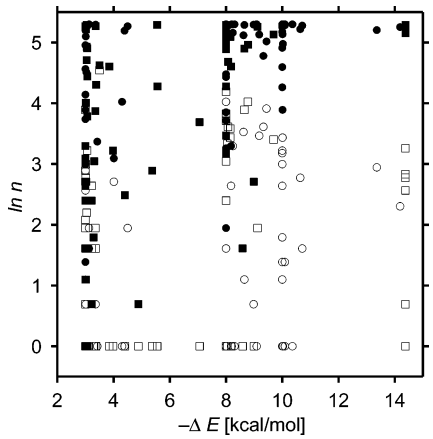

Figure 7. Scatter plots of the relationship between the logarithm of the number of structures without nativelike elements (empty symbols) and structures with at least one nativelike element (filled symbols), whose energy is within the standard energy gap from the lowest-energy non-native structure, as a function of the standard energy gap for model 1A (squares) and model 1B (circles).

pared to those of hierarchies M1H1 (empty squares in Figure 8). The reason for this is that structures with all contacts across the chain developed but with no other native contact need to be partially unfolded first to form all native turns because the adopted set of moves does not include the bending of the long hairpin in the middle in a single step. Obviously, in reality, all motions of a polypeptide chain are highly cooperative, and the bending of a long hairpin into the minimal β-barrel can easily occur without the partial unfolding of the hairpin. This observation implies that artificial barriers introduced by a search method implemented to generate a decoy set for potential-function optimization will affect the resulting potentials in that optimization will be directed at overcoming artificial energy barriers induced by a particular search method. This means that one must carefully select the search method to generate the decoy set to obtain a physics-based potential function to avoid the appearance of artificial barriers; the best search procedures from this viewpoint appear to be the molecular dynamics method and the force-biased Monte Carlo method.

When analyzing the trajectories of the simulated folding, we realized that one of the native turns (stabilized by a hydrophobic contact) is formed first and then structures with the central turn and one side turn develop, which is followed by the formation of structures with the complete hydrophobic cage that finally folds easily into the native structure. Therefore, in the next series of calculations, we assumed hierarchy M1H3 (Figure 5), which reflects the natural sequence of folding events. The results are summarized in Table 3 and Figure 8. It can be seen from Figure 8 that this hierarchy resulted in the highest τ_s^{max} values and, moreover, that the τ_s^{max} values are large even with small energy gaps between the native and the lowest-energy non-native structure.

Nonhierarchical and Hierarchical Optimization with Model 1B. Because the formation of turns facilitates the folding, in model 1B we introduced glycine residues into the turn positions to facilitate turn formation and carried out nonhierarchical and hierarchical optimizations. It can be seen from Table 3 and Figures 4 and 8 that this resulted in the largest τ_s^{max} and the lowest τ_f^{min} values. Moreover, for hierarchical optimization, excellent folders are obtained even when a small target energy gap between the native structure and the next structure is

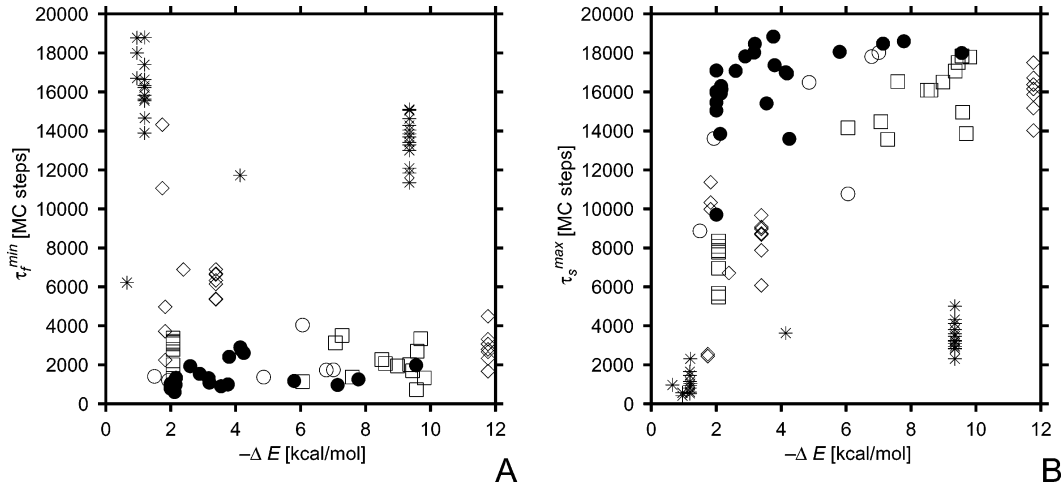

Figure 8. Scatter plots of the relationship between τ_f^{min} (A) and τ_s^{max} (B) with the standard energy gap (ΔE) for hierarchical optimizations of models 1A and 2A. Empty squares: hierarchy M1H1, model 1A; empty diamonds: hierarchy M1H2, model 1A; empty circles: hierarchy M1H3, model 1A; filled circles: hierarchy M1H3, model 1B; asterisks: reversed hierarchy M1H1, model 1A.

TABLE 4: Values of Target Energy (Δ) and *Z*-Score (ζ) Gaps and the Ranges of Initial Parameters for Models 2A and 2B

			Δ[c] (kcal/mol)				ζ[c]				ϵ_{HP}	ϵ_{PP}	ϵ_{el}	e_{bend}	
model	hierarchy[a]	set[b]	0−1	1−2	2−2	3−4	0−1	1−2	2−3	3−4	(kcal/mol)	(kcal/mol)	(kcal/mol)	(kcal/mol)	w_{tor}
2A	none	1	20.0				2.0				[−10...10]	[−10...10]	[−10...10]	[−10...10]	[−10...10]
		2[d]	20.0				2.0				[−10...10]	[−10...10]	[−10...10]	[−10...10]	[−10...10]
2A	M2H1	1	2.0	2.0	2.0		1.5	1.5	1.5		[−10...10]	[−10...10]	[−10...10]	[−10...10]	[−10...10]
2A	M2H2	1	2.0	2.0	2.0		1.5	1.5	1.5		[−10...10]	[−10...10]	[−10...10]	[−10...10]	[−10...10]
2A	M2H3	1	2.0	2.0	2.0	3.0	1.5	1.5	1.5	2.0	[−10...10]	[−10...10]	[−10...10]	[−10...10]	[−10...10]
		2[d]	10.0	5.0	5.0	5.0	1.5	1.5	1.5	2.0	[−10...10]	[−10...10]	[−10...10]	[−10...10]	[2...10]
		3[d]	20.0	2.0	2.0	3.0	1.5	1.5	1.5	2.0	[−10...10]	[−10...10]	[−10...10]	[−10...10]	[2...10]
2B	none	1[d]	20.0				2.0				[0...3]	[−2...3]	[−2...1]	[−2...2]	[2...5]
2B	M2H1	1[d]	2.0	2.0	2.0		1.5	1.5	1.5		[0...3]	[−2...3]	[−2...1]	[−2...2]	[2...5]
2B	M2H2	1[d]	2.0	2.0	2.0		1.5	1.5	1.5		[0...3]	[−2...3]	[−2...1]	[−2...2]	[2...5]
2B	M2H3	1[d]	2.0	5.0	2.0	2.0	1.5	1.5	1.5	1.5	[0...3]	[−2...3]	[−2...1]	[−2...2]	[2...5]

[a] See the text and Figure 5 for the description of hierarchies. [b] Denotes the number of the set of calculations for a given system (model and hierarchy) but different target energy and *Z*-score gaps. [c] Target energy and *Z*-score gaps (eq 4) between consecutive levels marked as $i - j$ for a gap between levels i and j, the highest level being the native level. For nonhierarchical optimizations, level 0 denotes all structures except native and level 1, the native structure. [d] The mirror image of the native structure moved to the native level and the differentiation of the native and the non-native structure achieved by imposing constraints on w_{tor}.

imposed (Figure 8). Even for nonhierarchical optimization, there are more good folders with a smaller standard energy gap than for model 1A. An analysis of the energy spectra shows that there are more states with native elements within the standard energy gap window (Figure 7). It can therefore be concluded that an appropriately designed local-interaction pattern not only improves the folding properties but also induces level ordering even if not imposed explicitly.

3.2. Models 2A and 2B. As mentioned in section 2.3, models 2A and 2B have unique native structures with the potential used. The native structure of model 2A (and, correspondingly, model 2B) is distinguished from its mirror image because of different values of U_{tor} of eq 3. It can therefore be supposed that local interactions play a much greater role here than for models 1A and 1B. The settings for the calculations are summarized in Table 4, and the results are summarized in Table 5.

We started from the nonhierarchical optimization of model 2A, setting a large target energy gap between the native structure and the lowest-energy non-native structure, which in most cases turned out to be the mirror image of the native structure. Given the constraints imposed on the parameters, the maximum attained energy gap was 2.5 kcal/mol. The results are summarized in Table 5. As for models 1A and 1B, the results differ both in τ_f^{min} and in τ_s^{max}. The results are clearly inferior to those achieved for models 1A and 1B, which is caused primarily by the fact that the native structure is now nondegenerate and it is therefore less probable to find it.

Next, we carried out hierarchical optimizations. In contrast to model 1A, an arbitrary construction of structural levels to build hierarchy M2H1 (Figure 9), in which level 1 contains structures with a single side, and level 2, structures with two sides formed, does not help foldability; in fact, the best result of hierarchical optimization is far worse than the best result of nonhierarchical optimization (Table 5). Next, we tried hierarchy M2H2 (Figure 9), in which the formation of the central loop stabilized by a hydrophobic contact is assumed to occur first, which is followed by the formation of all contacts between the two sides. However, the results are only comparable to those of nonhierarchical optimization (Table 5).

An analysis of most of the folding trajectories revealed that the mirror image of the native structure is often reached first. Therefore, the system often gets stuck in the mirror image at low temperature, and if the temperature is too high, the native structure is not stable enough. To satisfy these two contradictory requirements, we designed hierarchy M2H3 (Figure 9), in which the conversion between the mirror images is facilitated. The

TABLE 5: Summary of the Results of Monte Carlo Simulations with Optimized Potential-Function Parameters for Models 2A and 2B

model[a]	hierarchy[a]	set[a]	NP[b]	$\theta(\tau_s^{max})$[c]	$\tau_f(\tau_s^{max})$[c]	τ_s^{max} [c]	$\theta(\tau_f^{min})$[c]	τ_f^{min} [c]	$\tau_s(\tau_f^{min})$[c]
				3.00	6968	6486	5.00	2148	971
		1	20	4.00	15 807	1288	6.00	11 682	964
				4.60	10 524	3162	5.15	4927	1049
2A	none			3.50	7773	11 455	6.00	2033	3256
		2[d]	40	5.00	13 325	4670	7.00	7584	1717
				6.00	10 109	8172	6.33	3682	2928
				2.40	13 182	3195	4.00	7831	458
2A	M2H1	1	3	1.80	16 277	8	1.80	16 277	8
				3.93	13 293	2055	4.27	11 451	443
				2.40	6568	6016	4.00	2087	1384
2A	M2H2	1	20	1.80	12 962	21	1.80	12 962	21
				3.42	10 105	3673	3.70	4592	1388
		1	1	2.40	3057	8435	3.00	1636	5431
				1.20	10 493	9474	4.00	1905	2846
		2[d]	2	2.40	13 312	2158	4.00	8848	114
2A	M2H3			3.75	11 903	5816	4.00	5376	1480
				3.00	8718	10 258	5.00	2535	4670
		3[d]	2	3.00	9032	10 193	6.00	3672	1267
				5.50	8875	10 225	5.50	3103	2968
				1.20	3492	13 773	1.80	1124	3534
2B	none	1[d]	20	1.20	5829	9197	1.80	2552	3565
				1.71	5594	11 728	1.77	1820	4000
				0.80	11 159	7710	0.40	1551	800
2B	M2H1	1[d]	2	0.40	1551	800	1.80	2974	1467
				1.10	6355	4255	1.10	2263	1133
				0.40	4487	13 705	0.80	1601	11348
2B	M2H2	1[d]	2	0.80	11 774	8026	1.80	3759	1015
				1.00	8130	10 866	1.30	2680	6182
				0.60	2624	14 664	1.20	998	3172
2B	M2H3	1[d]	20	0.40	9022	8860	1.20	3251	1473
				0.81	5541	12 304	1.08	1814	4544

[a] See the legend to Table 4 for an explanation. [b] Number of different sets of energy-function parameters obtained in optimization. [c] See eqs 11 and 12 and the text of section 2.3 for definitions of these quantities. If more than one set of parameters was obtained for given settings, the results are presented in three consecutive rows. The upper row contains the best results in terms of τ_s^{max} (columns 5−7) and τ_f^{min} (columns 8−10), the middle row, the worst results in terms of τ_s^{max} and τ_f^{min}, and the third row, the averages over all sets of parameters. [d] The mirror image of the native structure moved to the native level, and the differentiation of the native and the non-native structure was achieved by imposing constraints on w_{tor}.

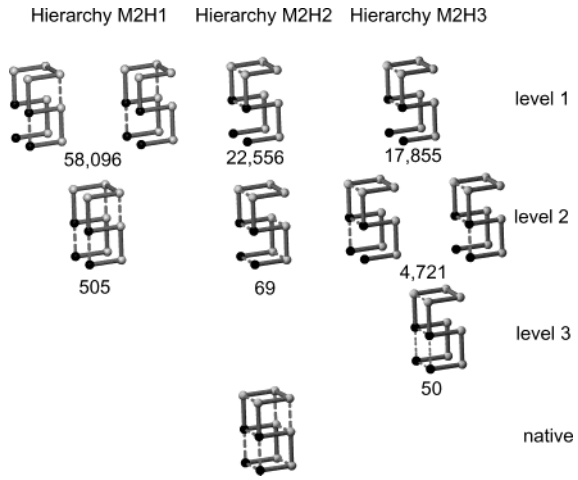

Figure 9. Illustration of the hierarchy levels of models 2A and 2B for hierarchies M2H1, M2H2, and M2H3 (c). The structures classified to given levels are requested to possess the native contacts shown in the pictures. The contacts are shown on the scaffold of the native structure.

first level is the same as in hierarchy M2H2; however, the second level consists of structures with additionally one of the terminal turns formed and attached to the central loop with a hydrophobic contact and the third level having both terminal turns and all four hydrophobic contacts developed. Thus, structures of level 3 already have the complete hydrophobic core, but the contacts between the other residues are not required to be particularly strong so that interconversion, which can occur most easily by three consecutive crankshaft moves of turns at residues 1−4, 5−8, and 9−12 (Figure 2), is facilitated. The results in Table 5 confirm that this hierarchy gives reasonably good folders.

The side effect of forcing a large energy gap between the native structure and the lowest-energy non-native structure (effectively its mirror image) was that the parameters drifted to result in large total (negative) energies (even below −100 kcal/mol for the lowest-energy structures). For such a small system, these energies are clearly unphysical. Although the system studied is very simple, it captures the frequently occurring real situation for which there are two stable structures that are mirror images of each other (e.g., a three-helix bundle) and the one that is marginally stable is the native structure, whereas the other one is not found experimentally. Of course, in such cases, forcing a maximum energy gap between the two mirror images is not a good idea; rather, one should ensure the stability of contacts between the components and a low-energy interconversion path between the two mirror-image structures. This has much in common with the concept of buffed energy landscapes introduced recently by Plotkin and Wolynes.[46] Therefore, in the next round of runs, we included the mirror image in the same level as the native structure but put appropriate constraints on

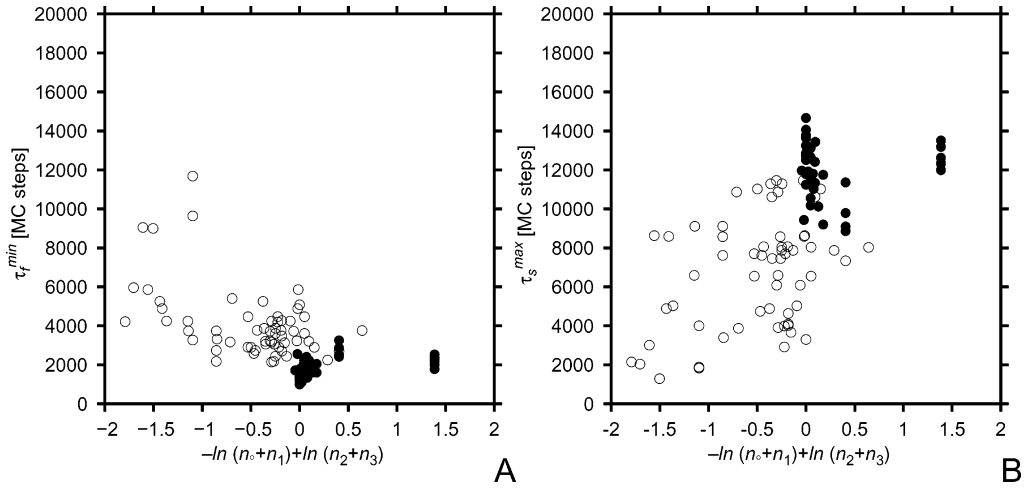

Figure 10. Scatter plots of the relationship between τ_f^{min} (A) and τ_s^{max} (B) of models 2A (empty circles) and 2B (filled circles) and the difference in the logarithm of the occupancy of levels 2 and 3 and levels 0 and 1 within the standard energy gap.

the weight of the torsional energy (w_{tor} in eq 3) to provide $\Delta E \geq 0.5$ kcal/mol between the mirror image and the native structure. We carried out both nonhierarchical optimization and hierarchical optimization with hierarchy M2H3. It can be seen (Table 5) that for both hierarchical and nonhierarchical optimization the lowest τ_f^{min} is several times smaller and τ_f^{max} is several times larger than in previous optimizations. The results now resemble those for model 1A with a small target energy gap: for hierarchical optimization, foldability depends on the energy gap between the native structure and the next level (which does not include the mirror image), whereas the results of nonhierarchical optimization span from poor to good folders. As for model 1A, an analysis of the energy spectra of the system obtained by nonhierarchical optimization indicates that good folders appear only where level ordering has been achieved.

To improve foldability, we redesigned the sequence to distinguish the mirror images better by energy and to facilitate the formation of the turns that are crucial for the formation of native contacts and the facility of interconversion between the mirror images; the resulting model is referred to as model 2B. A systematic analysis of torsional potentials showed that the energy difference between the native structure and its mirror image is increased when the central glycine residues are shifted one position forward; this makes the mirror image of model 2A the native structure of model 2B. To facilitate the formation of the turns, we introduced glycine residues into the terminal turns. The mirror image was assigned to the native level, and the differentiation of the mirror image from the native was achieved by appropriate constraints on w_{tor}. We carried out both nonhierarchical optimizations and hierarchical optimizations with hierarchies M2H1, M2H2, and M2H3. It can be seen from Table 5 that nonhierarchical optimization and optimization with hierarchy M2H3 give comparable results. However, an analysis of the energy spectra of the systems obtained even in nonhierarchical optimization shows that the levels are ordered following hierarchy M2H3. It is interesting that good results were also obtained with hierarchy M2H2; this is caused by the fact that the sequence was designed to facilitate turn formation and the terminal turns are, therefore, low in energy without explicitly requiring this by level ordering. However, hierarchy M2H2 does not guarantee low barriers to interconversion between the mirror images; therefore, the results are slightly worse than those obtained with hierarchy M2H3. Using the arbitrary hierarchy M2H1 gives results clearly inferior to those with hierarchy M2H3 and nonhierarchical optimization.

As for models 1A and 1B, we tried to find a single quantity that could be linked to the foldability of a system. We found some correlation of τ_f^{min} and τ_s^{max} with the difference in the logarithms of the occupancies of levels 2 and 3, and levels 0 and 1, of hierarchy M2H3. The respective scatter plots are shown in Figure 10. It can be seen that the correlation is less tight than that of Figure 4G and H. There is no correlation between the sum of the standard energy gap and the difference of the scaled entropy of the structure with and without nativelike elements. This means that the folding time and the stability of the native structure are somehow related to the difference in the occupancy of states with different nativelikeness that have energy similar to that of the native structure, but it is not obvious which degree of nativelikeness should be chosen. This, in turn, suggest that foldability cannot be related to a single quantity characterizing a system.

3.3. Relationship between C_v, χ, and Level Ordering. In what was presented thus far (sections 3.1 and 3.2), we demonstrated that neither the energy gap nor the Z score uniquely determines the folding rate or the stability of the native state and that appropriate ordering of the energy levels corresponding to increasing nativelikeness is necessary for a good folder. A question that can be asked, however, is whether there is a single quantity that captures this appropriate ordering of the energy levels and could, therefore, be a unique criterion of foldability. Quite recently, Thirumalai and co-workers[25,42−44,47] found that the quantity σ, defined by eq 13, is very well correlated with folding rates for lattice models; this observation was later generalized to off-lattice chains[47]

$$\sigma = \frac{T_c - T_f}{T_c} \tag{13}$$

where T_c is the collapse-transition temperature identified as that of the peak on the $C_v(T)$ curve,[42] with C_v being the constant-volume heat capacity of the system defined by eq 14, when passing from high to low temperatures and T_f is the folding temperature defined as that of the peak on the $\langle\chi(T)^2\rangle - \langle\chi(T)\rangle^2$ (fluctuations of χ) curve, with χ being the average overlap with the native structure, which for simple lattice models is defined by eq 15.

$$C_v(T) = \langle E^2 \rangle_T - \langle E \rangle_T^2 \tag{14}$$

$$\chi(T) = \langle \chi \rangle_T \tag{15}$$

$$\chi_i = 1 - \frac{1}{(n-1)(n-2)} \sum_{k,l;|l-k|>1} \delta(d_{kl}^i - d_{kl}^N) \tag{16}$$

$$\delta(x) = \begin{cases} 1 & \text{if } x = 0 \\ 0 & \text{otherwise} \end{cases} \tag{17}$$

where $\langle \cdots \rangle_T$ denotes a canonical average at absolute temperature T (see eq 8 for definition), d_{kl}^i and d_{kl}^N are the distances between residues k and l in conformation i and in the native structure, respectively, and the δ function is the Kronecker symbol.

The authors found that for lattice models with contact-only potentials σ is well correlated with the folding time and can therefore be considered to be a quantitative criterion of foldability.[25,42−44] We therefore determined the curves $C_v(T)$ and $\langle \chi(T)^2 \rangle - \langle \chi(T) \rangle^2$ for the systems studied and calculated the σ values. When multiple peaks or peaks and inflection points were present in the curves, we calculated the weighted averages of their positions as in ref 42. The scatter plots of τ_f^{min} as functions of σ for models 1A and 1B are shown in Figure 11A, and those for models 2A and 2B, in Figure 11B. It can be seen that the relationship resembles that between the standard energy gap and τ_f^{min} of Figure 4A: with large σ, τ_f is larger (slow folders), but for small σ, any values of τ_f can be obtained. Eliminating folders with low stability ($\tau_s^{max} < 10\,000$) from the data does not improve the correlation. It should be noted, however, that Thirumalai and co-workers reported tight correlation only for systems with sufficient stability of the native state, and they defined τ_f as the mean first passage time (MFPT) at T_f and not the lowest MFPT over all temperatures as in this work (eq 11). Moreover, their energy function did not contain contributions from local or electrostatic interactions. Furthermore, the data in Figure 11 correspond to different folding temperatures. When analyzing the $C_v(T)$ and $\langle \chi(T)^2 \rangle - \langle \chi(T) \rangle^2$ curves of various folders, we noticed, however, that particularly poor folders are often characterized by noncoinciding peaks in the $C_v(T)$ and $\langle \chi(T)^2 \rangle - \langle \chi(T) \rangle^2$ curves or even by two peaks or a peak and a saddle point in these curves, although one must be cautious in interpreting these features. Such folders include model 1A optimized in the non-hierarchical mode or with hierarchy M2H1 (which gave worse results than nonhierarchical optimization) and model 1A optimized by forcing the reversal of the hierarchy. To illustrate this, sample curves calculated for good and bad folders of model 1A are shown in Figure 12. It can be seen that the discrepancy between the peaks might indicate the incompatibility of the energy-level ordering with the pathway to the native structure. This can be explained as follows: At high temperatures, all conformations contribute equally to the averages. When the temperature is lowered and lower-energy conformations start to gain more significant weight, the average energy first shows a large change when a high concentration of energy levels first appears. This can also correspond to a significant increase in the nativelikeness; therefore, a jump in χ can also be observed at a comparable temperature if the increase in nativelikeness follows the decrease in energy. If the energy levels are ordered following the nativelikeness, then these jumps continue until the folding temperature is reached. If, however, the ordering of levels does not follow the pathway to the native structures, then a plateau in both curves can be expected after the first jump, which will continue until the temperature is low enough for only the native and very near native structures to have significant weight. In such a case, the energy landscape can be expected to be very rugged on the way to the native structure, and there will be significant barriers to folding. This explanation is similar to that given by Thirumalai and co-workers.[25,42−44] It is interesting that for models 1B and 2B where the sequence was designed to provide compatibility of the local interactions with the folding pathway the curves $C_v(T)$ and $\langle \chi(T)^2 \rangle - \langle \chi(T) \rangle^2$ each have a single peak at the same or nearly the same temperature (low σ values; Figure 11). It can thus be concluded that the analysis of the $C_v(T)$ and $\chi(T)$ curves can provide useful information as to the appropriateness of the hierarchy applied. However, the overlap function χ should be revised to include information about chirality; in its present form, it cannot distinguish the native structure from its mirror image.

It should be noted, however, that Figures 11 and 12 also show that the shapes of the $C_v(T)$ and $\langle \chi(T)^2 \rangle - \langle \chi(T) \rangle^2$ curves do not uniquely determine the appropriateness of the hierarchy. First, small values of σ do not seem to guarantee rapid folding. The curves of Figure 12D demonstrate that the maxima in the C_v and $\langle \chi(T)^2 \rangle - \langle \chi(T) \rangle^2$ curves can nearly coincide even for a bad folder. The explanation for this is that the system illustrated in

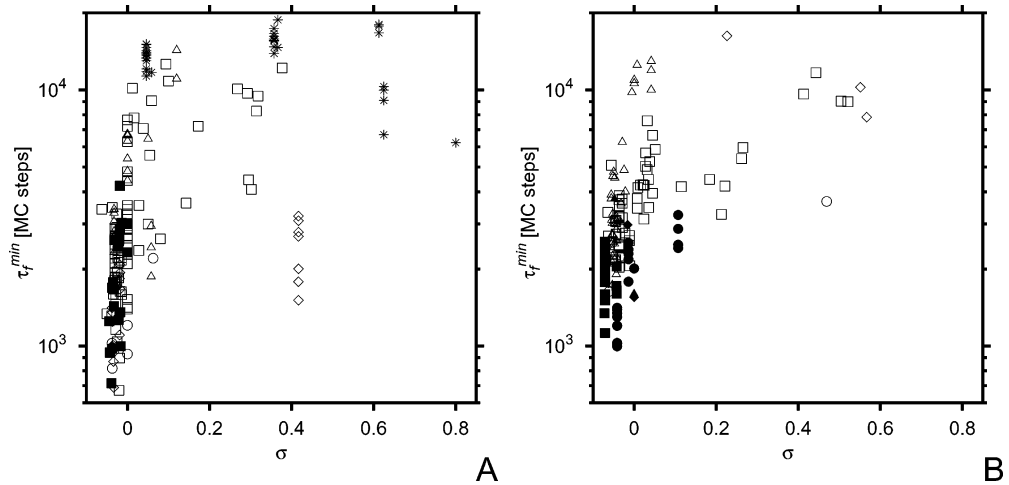

Figure 11. Scatter plots of the dependence of τ_f^{min} on the parameter σ (eq 13) for models 1A and 1B (A) and for models 2A and 2B (B). A logarithmic scale is applied to τ_f^{min}. Empty symbols, models 1A and 2A; filled symbols, models 1B and 2B; squares, non-hierarchical optimization; diamonds, hierarchies M1H1 and M2H1; triangles, hierarchies M1H2 and M2H2; circles, hierarchies M1H3 and M2H3; asterisks, reversed hierarchy M1H1.

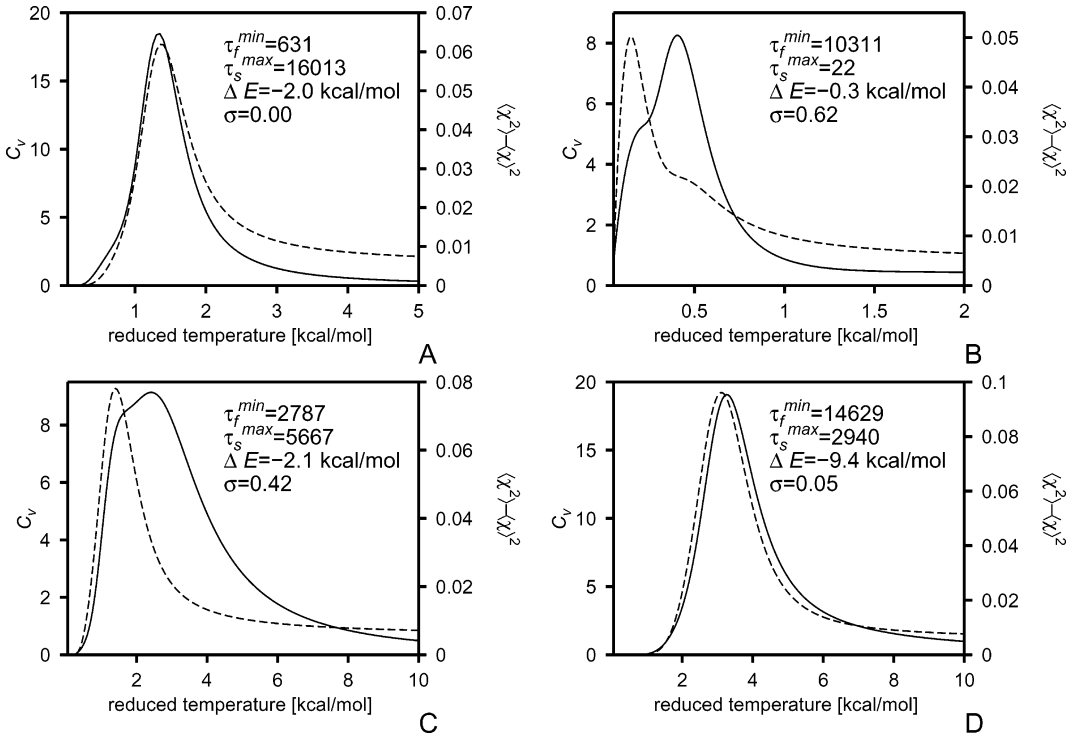

Figure 12. Sample curves of the temperature dependence of the heat capacity ($C_v(T)$; solid lines) and the fluctuations of the similarity to the native structure ($\langle\chi(T)^2\rangle - \langle\chi(T)\rangle^2$; dashed lines) for different folders of model 1A. (A) Good folder obtained with hierarchical optimization with hierarchy M1H1. Each of the two curves has one maximum at the same position. (B) Bad folder obtained by optimization with reversed hierarchy M1H1. Each curve has a maximum and an inflection point, and the maximum of $\langle\chi(T)^2\rangle - \langle\chi(T)\rangle^2$ occurs at lower temperature than that of C_v; this means that the major drop in mean energy occurs before the transition to the native structure occurs. (C) Moderate folder obtained by hierarchical optimization with hierarchy M1H1. The positions of the maxima are related as in panel B, but this is caused not by the misordering of the energy levels but by the sparseness of the energy spectrum in the near-native region. (D) Bad folder obtained by optimization with reversed hierarchy M1H1 with a large target energy gap between the native structures and the lowest-energy non-native structure. Despite the fact that the system is a bad folder, the maxima of the two curves nearly coincide because the change in the average energy and χ is dominated by the low energy of the native structures, which dominates in the averages. The values of τ_f^{min}, τ_s^{max}, σ, and ΔE are printed on each graph for better comparison. It should be noted that with the reduced temperature expressed in energy units the heat capacity is dimensionless.

Figure 12D has a large standard energy gap; therefore, the energy of the native structure dominates in the averages. The curves shown in Figure 12C, in turn, demonstrate that the peaks in the $C_v(T)$ and $\langle\chi(T)^2\rangle - \langle\chi(T)\rangle^2$ curves are divergent and, moreover, that the $C_v(T)$ curve does have structure, even though the corresponding system is a relatively fast (though a less-stable) folder. This can be explained if we recall that although this system corresponds to hierarchical optimization the energy spectrum is sparse relative to the standard energy gap (such as that shown in Figure 6B). These findings demonstrate that one must be cautious when linking the features of $C_v(T)$ and $\langle\chi(T)^2\rangle - \langle\chi(T)\rangle^2$ to the correspondence between energy and nativelikeness. It can also be concluded that because of the lack of full correspondence between σ and the energy-level ordering according to nativelikeness the minimization of σ cannot be considered to be an alternative for hierarchical optimization.

The observation that the folding rates can differ significantly for small σ values conforms with the results of a recent study of Plaxco and co-workers,[48] in which the authors measured the σ values experimentally for AcP, protein L, lysozyme, ubiquitin, and cytochrome *c*, which span a folding rate from 0.22 to 6300 s^{-1}. The collapse (T_c) temperature of eq 13 was determined as the temperature at which the radius of gyration of the ensemble of conformations is the arithmetic average of the radius of gyration of the unfolded and folded structure, and the folding temperature (T_f) was determined as that at which half of the ensemble is in the folded state. The radius of gyration was monitored by small-angle X-ray scattering (SAXS), whereas the progress of folding, by UV CD spectroscopy. For all five proteins studied, the measured σ values ranged from −0.02 to 0.05, despite major differences in the folding rates of these proteins.[48]

4. Conclusions

Using simple lattice protein models with enumerable conformational space, we compared the hierarchical optimization algorithm proposed in our previous work[11] with energy-gap and *Z*-score optimization.[6,9,15−23,28−31] We found that optimizing the energy gap between the native structure and the non-native structures and the *Z* score does not guarantee good folding properties even for the simple model system studied in this work. The folding time and stability of the native structure are not directly correlated with the energy gap, no matter how the energy gap is defined, or with the *Z* score. However, there seems to be good correlation between the stability of the native structure and the sum of the energy gap and the difference between the entropy of the structure with nativelike and those without nativelike elements.

When an appropriate ordering of energy levels is introduced according to the degree of nativelikeness of the corresponding structures, the folding time decreases significantly, and the stability increases with an increasing energy gap between the native level and the next level. Conversely, forcing the ordering of non-native energy levels opposite to nativelikeness results in poor folders even when the energy gap between the native

structure and the next structure is high. Forcing the compactness of the lowest non-native levels by requiring a large energy and *Z*-score gap between the compact and noncompact conformations can impair foldability. That energy-level ordering is important even for the simple models studied here strongly suggests that hierarchical optimization and not just energy-gap and *Z*-score optimization, understood as differentiating the native structure from non-native structures independent of the degree of nativelikeness of the latter, is absolutely necessary for real proteins, and no single quantity characterizing the bulk of non-native states is a good substitute for the explicit inclusion of energy-level ordering into optimization.

The design of a structural hierarchy is very important for foldability, and the best hierarchy should involve not only an increase in the number of nativelike elements with decreasing energy but also the order in which they appear. A wrong order can give worse results than those of nonhierarchical optimization. This suggests that the recently introduced concept of funnel sculpting,[29,31] in which the target of optimization is increasing nativelikeness with decreasing energy but not any given order in which the nativelike elements are stabilized with decreasing energy, may not be an alternative to hierarchical optimization. The results presented in this paper suggest that the hierarchy should be constructed by following the shortest path to the native structure and should reduce the barriers between possible intermediates (such as the mirror image of the native structure).

An analysis of the dependence of the heat capacity and the fluctuations of the average overlap with the native structure on temperature suggests that they can indicate significant incompatibility in energy-level ordering with nativelikeness and, therefore, energy functions characteristic of poor folders; if the ordering of the energy levels does not follow the nativelikeness or if the structural hierarchy is badly designed, then the curves of C_v and $\langle\chi^2\rangle - \langle\chi\rangle^2$ will have two peaks, or the position of the peak in the derivative of the overlap function will occur at significantly lower temperatures than that in the heat-capacity curve. Therefore, the quantity σ introduced by Thirumalai and co-workers,[25,42−44,47] defined as the relative difference in the positions of the two peaks, can be a good indicator of the goodness of the hierarchy. However, small values of σ also occur for bad folders with violations of the ordering of levels, and it also follows from experiment[48] that small values of σ do not imply fast folding. Therefore, the optimization of σ may not be an alternative to hierarchical optimization.

Acknowledgment. This work was supported by grants from the National Institutes of Health (GM-14312), the National Science Foundation (MCB00-03722), the NIH Fogarty International Center (TW1064), and grant 3 T09A 032 26 from the Polish State Committee for Scientific Research (KBN). This research was conducted by using the resources of (a) our 392-processor Beowulf cluster at Baker Laboratory of Chemistry and Chemical Biology, Cornell University, (b) the National Science Foundation Terascale Computing System at the Pittsburgh Supercomputer Center, (c) our 45-processor Beowulf cluster at the Faculty of Chemistry, University of Gdańsk, (d) the Informatics Center of the Metropolitan Academic Network (IC MAN) in Gdańsk, and (e) the Interdisciplinary Center of Mathematical and Computer Modeling (ICM) at the University of Warsaw.

References and Notes

(1) Vásquez, M.; Némethy, G.; Scheraga, H. A. *Chem. Rev.* **1994**, *94*, 2183−2239.
(2) Anfinsen, C. B. *Science* **1973**, *181*, 223−230.
(3) Liwo, A.; Pincus, M. R.; Wawak, R. J.; Rackovsky, S.; Scheraga, H. A. *Protein Sci.* **1993**, *2*, 1697−1714.
(4) Liwo, A.; Pincus, M. R.; Wawak, R. J.; Rackovsky, S.; Scheraga, H. A. *Protein Sci.* **1993**, *2*, 1715−1731.
(5) Liwo, A. Ołdziej, S.; Pincus, M. R.; Wawak, R. J.; Rackovsky, S.; Scheraga, H. A. *J. Comput. Chem.* **1997**, *18*, 849−873.
(6) Liwo, A.; Pincus, M. R.; Wawak, R. J.; Rackovsky, S.; Ołdziej, S.; Scheraga, H. A. *J. Comput. Chem.* **1997**, *18*, 874−887.
(7) Liwo, A.; Kaźmierkiewicz, R.; Czaplewski, C.; Groth, M.; Ołdziej, S.; Wawak, R. J.; Rackovsky, S.; Pincus, M. R.; Scheraga, H. A. *J. Comput. Chem.* **1998**, *19*, 259−276.
(8) Liwo, A.; Czaplewski, C.; Pillardy, J.; Scheraga, H. A. *J. Chem. Phys.* **2001**, *115*, 2323−2347.
(9) Lee, J.; Ripoll, D. R.; Czaplewski, C.; Pillardy, J.; Wedemeyer, W. J.; Scheraga, H. A. *J. Phys. Chem. B* **2001**, *105*, 7291−7298.
(10) Pillardy, J.; Czaplewski, C.; Liwo, A.; Lee, J.; Ripoll, D. R.; Kańmierkiewicz, R.; Oldziej, S.; Wedemeyer, W. J.; Gibson, K. D.; Arnautova, Y. A.; Saunders, J.; Ye, Y.-J.; Scheraga, H. A. *Proc. Natl. Acad. Sci. U.S.A.* **2001**, *98*, 2329−2333.
(11) Liwo, A.; Arłukowicz, P.; Czaplewski, C.; Ołdziej, S.; Pillardy, J.; Scheraga, H. A. *Proc. Natl. Acad. Sci. U.S.A.* **2002**, *99*, 1937−1942.
(12) Lee, J.; Scheraga, H. A.; Rackovsky, S. *J. Comput. Chem.* **1997**, *18*, 1222−1232.
(13) Lee, J.; Scheraga, H. A. *Int. J. Quantum Chem.* **1999**, *75*, 255−265.
(14) Levinthal, C. *J. Chim. Phys. Phys.-Chim. Biol.* **1968**, *65*, 44−45.
(15) Goldstein, R. A.; Luthey-Schulten, Z. A.; Wolynes, P. G. *Proc. Natl. Acad. Sci. U.S.A.* **1992**, *89*, 9029−9033.
(16) Godzik, A.; Kolinski, A.; Skolnick, J. *J. Comput.-Aided Mol. Des.* **1993**, *7*, 397−438.
(17) Mirny, L. A.; Shakhnovich, E. I. *J. Mol. Biol.* **1996**, *264*, 1164 1179.
(18) Hao, M.-H.; Scheraga, H. A. *J. Phys. Chem.* **1996**, *100*, 14540−14548.
(19) Hao, M.-H.; Scheraga, H. A. *Curr. Opin. Struct. Biol.* **1999**, *9*, 184−188.
(20) Pillardy, J.; Czaplewski, C.; Liwo, A.; Wedemeyer, W. J.; Lee, J.; Ripoll, D. R.; Arłukowicz, P.; Ołdziej, S.; Arnautova, Y. A.; Scheraga, H. A. *J. Phys. Chem. B* **2001**, *105*, 7299−7311.
(21) Hardin, C.; Eastwood, M. P.; Prentiss, M.; Luthey-Schulten, Z.; Wolynes, P. G. *J. Comput. Chem.* **2002**, *23*, 138−146.
(22) Eastwood, M. P.; Hardin, C.; Luthey-Schulten, Z.; Wolynes, P. G. *J. Chem. Phys.* **2002**, *117*, 4602−4615.
(23) Eastwood, M. P.; Hardin, C.; Luthey-Schulten, Z.; Wolynes, P. G. *J. Chem. Phys.* **2003**, *118*, 8500−8512.
(24) Sali, A.; Shakhnovich, E.; Karplus, M. *Nature* **1994**, *369*, 248−251.
(25) Klimov, D. K.; Thirumalai, D. *J. Chem. Phys.* **1998**, *109*, 4119−4125.
(26) Crippen, G. M.; Snow, M. E. *Biopolymers* **1990**, *29*, 1479−1489.
(27) Seetharamulu, P.; Crippen, G. M. *J. Math. Chem.* **1991**, *6*, 91−110.
(28) Meller, J.; Elber, R. *Proteins: Struct., Funct., Genet.* **2001**, *45*, 241−261.
(29) Micheletti, C.; Seno, F.; Maritan, A.; Banavar, J. R. *Comput. Mater. Sci.* **2001**, *20*, 305−310.
(30) Lee, J.; Park, K.; Lee, J. *J. Phys. Chem. B* **2002**, *106*, 11647−11657.
(31) Fain, B.; Levitt, M. *Proc. Natl. Acad. Sci. U.S.A.* **2003**, *100*, 10700−10705.
(32) Maiorov, V. N.; Crippen, G. M. *J. Mol. Biol.* **1992**, *227*, 876−888.
(33) Derrick, J. P.; Wigley, D. B. *J. Mol. Biol.* **1994**, *243*, 906−918.
(34) Liwo, A.; Ołdziej, S.; Czaplewski, C.; Kozłowska, U.; Scheraga, H. A. *J. Phys. Chem. B* **2004**, *108*, 9421−9438.
(35) Ołdziej, S.; Liwo, A.; Czaplewski, C.; Pillardy, J.; Scheraga, H. A. *J. Phys. Chem. B* **2004**, 16934−16949.
(36) Ołdziej, S.; Łągiewka, J.; Liwo, A.; Czaplewski, C.; Chinchio, M.; Nanias, M.; Scheraga, H. A. *J. Phys. Chem. B* **2004**, 16950−16959.
(37) Chan, H. S.; Dill, K. A. *Proteins: Struct., Funct., Genet.* **1998**, *30*, 2−33.
(38) Kolinski, A.; Skolnick, J. *J. Chem. Phys.* **1992**, *97*, 9412−9426.
(39) Kondrak, G.; van Beek, P. *Artif. Intell.* **1997**, *89*, 365−387.
(40) Sali, A.; Shakhnovich, E. I.; Karplus, M. *J. Mol. Biol.* **1994**, *235*, 1614−1638.
(41) Shakhnovich, E. I. *Curr. Opin. Struct. Biol.* **1997**, *7*, 29−40.
(42) Camacho, C. J.; Thirumalai, D. *Europhys. Lett.* **1996**, *35*, 627−632.
(43) Klimov, D. K.; Thirumalai, D. *Phys Rev. Lett.* **1996**, *76*, 4070−4073.
(44) Klimov, D. K.; Thirumalai, D. *Proteins: Struct., Funct., Genet.* **1996**, *26*, 411−441.

(45) Scalley, M. J.; Yi, Q.; Gu, H.; McCormack, A., III; Yates, J. R.; Baker, D. *Biochemistry* **1997**, *36*, 3373−3382.
(46) Plotkin, S. S.; Wolynes, P. G. *Proc. Natl. Acad. Sci. U.S.A.* **2003**, *100*, 4417−4422.
(47) Thirumalai, D.; Klimov, D. K. *Curr. Opin. Struct. Biol.* **1999**, *9*, 197−207.
(48) Millet, I. S J. R.; Townsley, L. E J. R.; Chiti, F J. R.; Doniach, S.; Plaxco, K. W. *Biochemistry* **2002**, *41*, 321−325.